

Doublon Formation by Ions Impacting a Strongly Correlated Finite Lattice System

Karsten Balzer,¹ Maximilian Rodriguez Rasmussen,² Niclas Schlünzen,² Jan-Philip Joost,² and Michael Bonitz^{2,*}

¹Rechenzentrum, Christian-Albrechts-Universität zu Kiel, D-24098 Kiel, Germany

²Institut für Theoretische Physik und Astrophysik, Christian-Albrechts-Universität zu Kiel, D-24098 Kiel, Germany



(Received 17 January 2018; published 28 December 2018)

Strongly correlated systems of fermions have a number of exciting collective properties. Among them, the creation of a lattice that is occupied by doublons, i.e., two quantum particles with opposite spins, offers interesting electronic properties. In the past a variety of methods have been proposed to control doublon formation, both, spatially and temporally. Here, a novel mechanism is proposed and verified by exact diagonalization and nonequilibrium Green functions simulations—fermionic doublon creation by the impact of energetic ions. We report the formation of a nonequilibrium steady state with homogeneous doublon distribution. The effect should be particularly important for strongly correlated finite systems, such as graphene nanoribbons, and directly observable with fermionic atoms in optical lattices.

DOI: 10.1103/PhysRevLett.121.267602

Strongly correlated systems are attracting increasing interest in many fields including dense plasmas [1], warm dense matter [2], dusty plasmas [3], and ultracold atoms [4]. Among the most intriguing phenomena in strongly correlated quantum systems of both fermions and bosons is the formation of doublons—pairs of repulsively bound particles occupying the same lattice site [5]. In recent years, there have been many attempts to study the dynamics of doublons after a correlated system is driven out of equilibrium leading to many surprising results. “Quantum distillation”—the spatial separation of doublons and single fermions—was observed in Refs. [6,7]. The nonequilibrium expansion dynamics of a fermionic particle cloud following a confinement quench and its slowing down due to doublon formation has been studied experimentally in a 2D optical lattice [4] and theoretically by 2D quantum simulations using nonequilibrium Green functions (NEGF) [8]. Also, the external control of doublons by an interaction quench [9], by periodically modulating an optical lattice [10–12], by external electric fields [13–18] or by optical excitation [19] has been proposed. Furthermore, the dynamics of heteronuclear doublons [20] and the spatial transfer of doublons via topological edge states [21] have been studied.

Previous setups of doublon manipulation involved spatially homogeneous systems containing a large number of fermions triggering their collective response to a spatially delocalized excitation. In contrast, in this Letter we predict a novel mechanism to induce and control the formation of doublons in a finite system where the excitation is localized in space and time. The most interesting examples are finite graphene clusters (e.g., “nanoribbons,” GNR) that are fabricated in a controlled way, e.g., Refs. [22–24], and are accurately characterized experimentally [25–27]. In contrast to graphene, GNR have a finite band gap [28–30]

that can be tuned by varying the system size and geometry [31], giving rise to exciting electronic correlation effects and optical and transport properties [32]. The doublon excitation mechanism we are proposing is driven by energetic ions penetrating a strongly correlated finite system and depositing energy (“stopping power,” e.g., Refs. [33–36]). We demonstrate the mechanism by exact diagonalization simulations, and a physical explanation is given with an analytical model in terms of the Landau-Zener effect [37]. We then investigate how the doublon number depends on the cluster size in one and two dimensions by performing NEGF simulations and demonstrate the emergence of a stationary nonequilibrium state with homogeneous doublon distribution. Finally, we show that the effect can be further enhanced by using a sequence of excitations.

Model.—We consider strongly correlated electrons in a single-band finite Hubbard model containing L sites with nearest-neighbor hopping J and on-site interaction U ,

$$\hat{H} = -J \sum_{\langle i,j \rangle \sigma} \hat{c}_{i\sigma}^\dagger \hat{c}_{j\sigma} + U \sum_i \hat{n}_{i\uparrow} \hat{n}_{i\downarrow} + \sum_{i\sigma} W_i(t) \hat{n}_{i\sigma}, \quad (1)$$

where $\hat{n}_{i\sigma} = \hat{c}_{i\sigma}^\dagger \hat{c}_{i\sigma}$ is the density, σ denotes the spin, and $W_i(t) = -Ze^2/[4\pi\epsilon_0|\mathbf{r}(t) - \mathbf{r}_i|]$ describes the interaction of the electron at lattice site \mathbf{r}_i with a positive ion of charge Ze moving on a classical trajectory $\mathbf{r}(t)$, neglecting nonlocal contributions, $W_{ij} = \delta_{ij}W_i$. We denote $W_0 = e^2/(4\pi\epsilon_0 a)$ and measure energies, times, and lengths in units of J , $\hbar J^{-1}$, and the lattice constant a , respectively. The quantities of central interest are the site-resolved density, $n_{i\sigma}$, and double occupation d_i , the cluster average of d , and its long-time limit after passing of the projectile:

$$n_{i\sigma}(t) = \langle \hat{n}_{i\sigma}(t) \rangle, \quad d_i(t) = \langle \hat{n}_{i\uparrow}(t) \hat{n}_{i\downarrow}(t) \rangle, \quad (2)$$

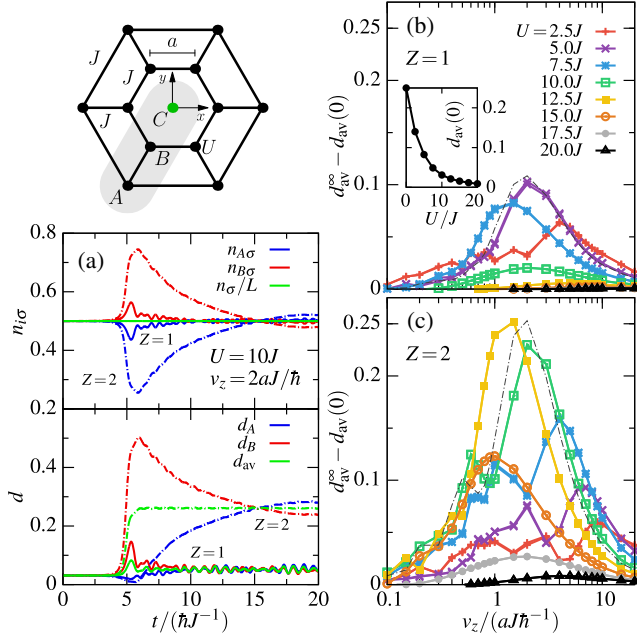


FIG. 1. Ion impact-induced doublon formation in a two-dimensional Hubbard nanocluster (top left, black points) with $L = 12$ sites, nearest-neighbor hopping J and on-site interaction U . (a) Time evolution of the electron density $n_{i\sigma}$ (top) and double occupation d_i (bottom) on sites A (blue) and B (red) for a positive charge with $Z = 1$ (solid lines) and $Z = 2$ (dash-dotted lines) impacting the system at $U = 10J$ with velocity $v_z = 2aJ/\hbar$ in point $C = (0, 0, 0)$. The green curves show the mean density, $n_{\sigma}(t)/L = (1/L) \sum_i n_{i\sigma}(t) = 0.5$, and double occupation $d_{av}(t)$, Eq. (3), respectively. (b) and (c) Increase of the double occupation, $d_{av}^{\infty} - d_{av}(0)$ [inset in (b) shows $d_{av}(0)$], as a function of v_z for different U and $Z = 1$ ($Z = 2$), where the thin dash-dotted gray curves correspond to $U = U^* = 5.4J$ ($U = U^* = 10.8J$), as derived from the dimer model below.

$$d_{av}(t) = \frac{1}{L} \sum_{i=1}^L d_i(t), \quad d_{av}^{\infty} = \lim_{t \rightarrow \infty} \frac{1}{\Delta t} \int_t^{t+\Delta t} \bar{d} \bar{t} d_{av}(\bar{t}). \quad (3)$$

Results for a finite 2D cluster.—In Figure 1, we present solutions of the system (1) for an exemplary 2D half-filled Hubbard nanocluster with $L = 12$ sites, obtained by time-dependent exact diagonalization (CI) starting at $t = 0$ from the ground state. The trajectory of the ion is set to $\mathbf{r}(t) = (0, 0, z + v_z t)$ with velocity v_z and initial z position such that $W_i(t=0) \rightarrow 0, \forall i$. We use $W_0 = 14.4J$, which corresponds to a force $J/a = 1$ eV/Å. Figure 1(a) shows the time evolution for an on-site interaction $U = 10J$, $v_z = 2aJ/\hbar$, and $Z = 1$ and 2 , where the expectation values are computed as $\langle \hat{O} \rangle(t) = \langle \psi(t) | \hat{O} | \psi(t) \rangle$, with the many-electron wave function $|\psi(t)\rangle = \{T \exp[-(i/\hbar) \int_0^t ds \hat{H}(s)]\} |\psi(0)\rangle$ and time-ordering operator T . During the time of impact ($t = 5\hbar/J$), both $n_{B\sigma}$ and d_B ($n_{A\sigma}$ and d_A) increase (decrease). After departure of the projectile the electron densities return (close) to their initial value $n_{i\sigma} = 0.5$.

In contrast, the spatiotemporal evolution of the double occupation [38] is such that $d_{A,B}$ remain above their initial value, particularly for $Z = 2$. Thus, the projectile has created a significant number of stable doublons, indicating the emergence of a stationary nonequilibrium (“prethermalized” [39,40]) state. This is quantified in Figs. 1(b) and 1(c) by the asymptotic value of the average double occupation, d_{av}^{∞} (3). A striking result is the nonmonotonic dependence of d_{av}^{∞} on the projectile velocity with a maximum around $v_z \sim (1 \dots 3)aJ/\hbar$. Moreover, also the dependence on U is nonmonotonic: d_{av}^{∞} exhibits a single maximum which is in the range of $U \sim 5J$, for $Z = 1$, and $U \sim 12J$, for $Z = 2$. Further, d_{av}^{∞} increases with the projectile charge. We note that in the present setup we consider a projectile with constant kinetic energy; for a discussion on the energy transfer see Ref. [35]. Also, reducing the hopping J between the A sites (along the edges of the cluster), does not significantly change the results [41].

Analytical model.—To understand the main mechanism of the doublon formation, we consider a Hubbard dimer at half-filling and develop a Landau-Zener (LZ) description [9,18,37]. The dimer is excited by a time-dependent energy $W(t) = -W_0 \exp[-t^2/(2\tau^2)]$ on one site, which well mimics the projectile. Here the interaction duration with the projectile $\tau > 0$ is inversely proportional to the projectile velocity v_z , and we use $W_0 = 2U$. In the basis $\{|\uparrow, \downarrow\rangle, |\downarrow, \uparrow\rangle, |\uparrow\downarrow, 0\rangle, |0, \uparrow\downarrow\rangle\}$, the Hamiltonian

$$\hat{H}_{\text{dimer}}(t) = \begin{pmatrix} W(t) & 0 & -J & -J \\ 0 & W(t) & J & J \\ -J & J & U + 2W(t) & 0 \\ -J & J & 0 & U \end{pmatrix}, \quad (4)$$

is straightforwardly diagonalized for all times.

Figure 2(a) shows the evolution of all four eigenenergies, $E_0 \leq E_1 \leq E_U \leq E_2$, (the explicit expressions are given in the Supplemental Material [41]) for $U = 10J$ as function of $W(t)$. Starting in the triplet ground state (E_0), for $t = -\infty$, the dimer undergoes a transition to the second excited state (E_U) via an avoided crossing with probability p when $W(t)$ is switched on sufficiently fast. Using a reduced two-level Landau-Zener picture, the probability that the dimer, for $t = +\infty$, remains in state E_U can be approximated by a twofold (forward-backward) passage of the avoided level crossing:

$$P_{E_0 \rightarrow E_U} = 2p(1 - p), \quad (5)$$

with the LZ transition probability for a single diabatic passage of the crossing (for details see Ref. [41]),

$$p(\tau; U) = \exp\left(-\frac{\pi e^{1/2} [\min_{W(t)} (E_U - E_0)]^2 \tau}{2\hbar W_0 |d(E_U - E_0)/dW|}\right). \quad (6)$$

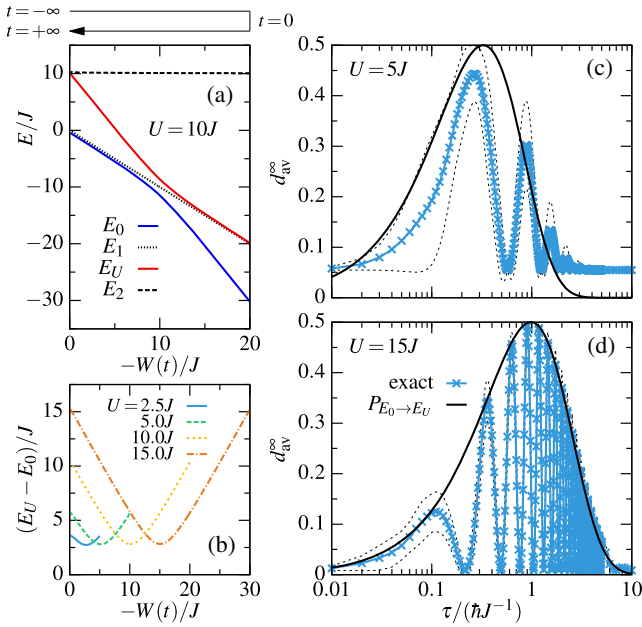


FIG. 2. Hubbard dimer of Eq. (4). (a) Evolution of the eigenenergies as a function of $W(t)$, for $U = 10J$. The initial and final state corresponds to $W = 0$, and the impact of the projectile to $-W/J = 20$; its trajectory is sketched above the figure. (b) Eigenenergy difference, $E = E_U - E_0$, as function of $W(t)$ for $W_0 = 2U$ and different values of U . (c) and (d) Asymptotic double occupation, for $U = 5J$ and $15J$ as function of τ . Blue: CI data [using $\Delta t = 50\hbar J^{-1}$ in Eq. (3)], black line: Landau-Zener result based on Eq. (5), thin dashed lines: exact minimum and maximum values of $d_{\text{av}}(t)$.

From Fig. 2(b), we observe that, around $W(t) = -W_0$, the level spacing and its derivative are almost independent of U ; therefore, the probabilities p and $P_{E_0 \rightarrow E_U}$ only depend (for fixed U) on the duration τ of the excitation.

Figures 2(c) and 2(d) show d_{av}^{∞} , in the dimer, for $U = 5J$ and $15J$ (black curves), together with the exact solution of Eq. (4). The most striking result is that d_{av}^{∞} can reach (and remain at) 0.5, for an optimal choice of τ , which is well captured by the LZ picture where this corresponds to the probability (6), $p = 1/2$, of creating a doublon on site one. Overall we observe that, for $U \gtrsim 10J$, our model (5) reproduces the envelope of $d_{\text{av}}^{\infty}(\tau)$ very well, although it does not capture the oscillations that are proportional to the field W_0 and are due to transient Bloch oscillations [43].

With insight from the dimer model, we find the parameters that maximize d_{av}^{∞} , in the 12-site cluster of Fig. 1: (i) the optimal interaction strength is $U^*/J \approx Z \times 5.4$; (ii) for $U = U^*$, the optimal velocity v_z^* decreases linearly with Z [41]. The result is shown by the thin gray dash-dotted line in Fig. 1(b) [Fig. 1(c)]. The striking agreement of the peak height and position with the CI result for $L = 12$ confirms that our model captures the correct physics: local doublon formation via a twofold passage of an avoided level crossing.

Maximizing the doublon number in larger 1D and 2D systems.—We now turn to finite Hubbard clusters with lower symmetry than the one in Fig. 1 starting with a 1D half-filled chain with $L = 8$ sites, $U = 20J$ and periodic boundary conditions which we solve exactly. To investigate how the spreading of the doublons along the chain changes compared to the dimer case we use the same local excitation, $W(t)$, applied only to site 1. As shown in Fig. 3(b), now the average doublon number reaches only $d_{\text{av}}^{\infty} \approx 0.08$, at $t \approx 15\hbar J^{-1}$. To increase d_{av}^{∞} further, we apply a second identical excitation to site one which indeed raises d_{av}^{∞} to 0.145. Repeating this procedure periodically allows for a successive increase until a value $d_{\text{av}}^{\infty} \approx 1/4$ is reached. This final value is consistent with the time evolution of the many-particle energy spectrum

$$S(\hbar\omega, t) = \sum_i |\langle \psi(t) | E_i \rangle|^2 e^{-\{(\hbar\omega - [E_i - UL/4])^2 / 2(\hbar\omega_0)^2\}}, \quad (7)$$

where $|E_i\rangle$ denote the energy eigenstates, which is shown in Fig. 3(c) for a level broadening $\hbar\omega_0 = J$. The final energy spectrum ($t > 200\hbar J^{-1}$) becomes symmetric around $\omega = 0$, therefore providing on average two doublons in the system, corresponding to $d_{\text{av}}^{\infty} \rightarrow 1/4$. Moreover, we observe that the double occupation (just as the density) becomes homogeneous along the chain, cf. Fig. 3(b), and

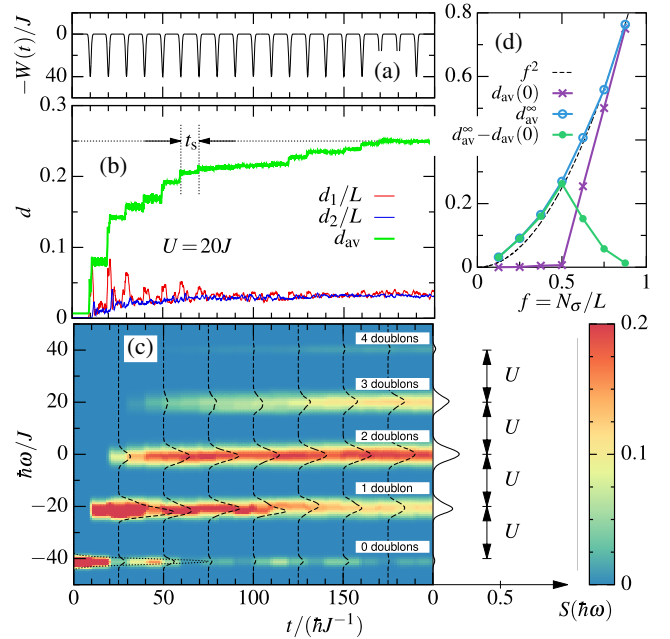


FIG. 3. Evolution of a half-filled Hubbard chain with $L = 8$ sites and $U = 20J$ subject to multiple excitations at site 1. (a) Applied field, $W(t)$, with $\tau = 0.5\hbar J^{-1}$ and peak separation $t_s = 10\hbar J^{-1}$. (b) Dynamics of the mean double occupation $d_{\text{av}}(t)$ of Eq. (3). (c) Time evolution of the energy spectrum $S(\hbar\omega, t)$, Eq. (7) with $\hbar\omega_0 = J$. (d) Doublon formation process for different filling fractions $f = N_{\sigma}/L$, where N_{σ} denotes the number of electrons of spin σ .

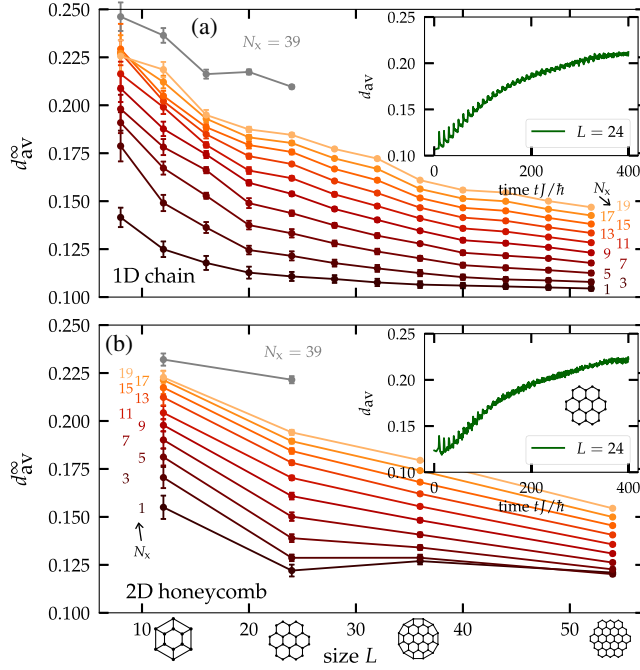


FIG. 4. Asymptotic double occupation (3) for (a) 1D chains and (b) 2D half-filled honeycomb clusters of different size L and $U = 4J$ from NEGF simulations. The number of excitations, N_x , which are performed on one of the innermost sites, is indicated in the figure. Insets show $d_{av}(t)$, for $L = 24$ and $N_x = 40$.

that the correlation part of the interaction energy vanishes almost completely [not shown], indicating the approach of a mean-field state. In Fig. 3(d), we furthermore investigate the same scenario for different fillings [44] ($N_{\sigma} = \sum_i n_{i\sigma} = 1, 2, \dots, 7$), which shows that the change of double occupation with respect to the initial ground state is largest for half-filling.

In order to test whether our doublon production protocol can be realized also in larger systems and 2D setups as well, we have performed extensive NEGF simulations for L up to 54 of long duration, $t \leq 400\hbar J^{-1}$, which enables us to consider up to $N_x = 39$ localized excitations of the same form as in Fig. 3(a). We used second-order Born self-energies within the generalized Kadanoff-Baym ansatz with Hartree-Fock propagators (HF-GKBA), as explained in detail in Refs. [8,35,45,46]. From benchmarks against density matrix renormalization group simulations [47] we expect that these simulations are reliable for $U/J \lesssim 4$. Tests against our present CI data for small systems confirm the high quality of the NEGF results and indicate that they yield a lower bound to d_{av}^{∞} , the exact result being 5%–15% higher.

In Fig. 4 we show the asymptotic double occupation, d_{av}^{∞} , for $W_0 = 2U = 8J$, for 1D chains, Fig. 4(a), and 2D honeycomb lattice fragments, Fig. 4(b). Clearly, the successive increase of d_{av}^{∞} with N_x is confirmed for larger systems. Also, for fixed N_x , we observe a decrease of d_{av}^{∞} with L , as expected. Extrapolating to larger values of N_x we expect that for all systems d_{av}^{∞} will reach at least 0.25.

Summary and discussion.—We have presented a novel scenario for the production of doubly occupied electronic states in correlated finite 1D and 2D Hubbard clusters that is based on the impact of energetic ions. We have reported CI results for system sizes $L \leq 12$ that were complemented by nonequilibrium Green functions simulations for $L \leq 54$. The physical mechanism has been made transparent by analytically solving the relevant dimer problem in the presence of an ion impact: it is the formation of avoided level crossings between bands of different doublon number, cf. Fig. 3, and it is straightforwardly extended to multiple sequential excitations. For the case that the system is not coupled to a bath [as in our simulations] we observed formation of a stationary homogeneous doublon population which provides another example for pre-thermalization phenomena [17,40,48,49] that recently have attracted high interest. More generally, we have presented a new scenario of nonequilibrium dynamics without thermalization [50,51] that is driven by a rapid, spatially localized single-particle potential quench instead of an interaction quench. While in the homogeneous state we observe doublon occupations up to 0.25, as in previous homogeneous excitation scenarios, e.g., Refs. [11–18], we have shown [cf. Figs. 2(c) and 2(d)] that, for inhomogeneous states in finite systems, significantly higher final values can be achieved. Moreover, the flexibility of the excitation protocol should allow for further optimization. We have verified (see Fig. 1 and Ref. [41]) that the same protocol can be realized also with Coulomb interaction where the long range interaction even enhances the doublon number.

Our results are directly applicable to finite correlated solid state systems, such as graphene nanoribbons [23–31], that are exposed to energetic ions [36]. For moderately correlated systems with typical parameters $J = 1$ eV and $a = 1$ Å, ion velocities $v_z \sim 1aJ/\hbar$ are required which translates into kinetic energies of 120 eV (480 eV) for protons (alpha particles). These values are well feasible with ion guns or in low-temperature high-pressure plasmas [52], where the present effect should have a strong influence on the stopping power [33–35] and may offer new optical and transport applications. Of course, for the case of multiple excitations, one would need to consider spatial variations of the impact point, energy, and time delay between impacts. These issues are easily studied within the dimer model and with our NEGF approach as well. Furthermore, for these systems the coupling to the environment (bath) and the associated dissipation effects will have to be included, which sets an upper limit for the lifetime of the nonequilibrium doublon state in the range of several hundred femtoseconds. Since the timescale of the doublon formation is of the order of 1–10 fs we expect that the presented scenario of multiple ion impacts can be realized.

Suitable candidates to verify this scenario experimentally are fermionic atoms in optical lattices. While direct ion impact will be less efficient, due to the weaker short range

charge-atom interaction [53], a promising approach is to mimic the projectile dynamics via suitable time-dependent local variation of the lattice potentials [54]. This would open the way to simulate, with cold atoms, ion stopping in condensed matter, including correlated materials.

We thank S. Kuhr for valuable information on the experimental issues related to Ref. [54]. This work was supported by HPC resources of Grant No. shp00015 at the North-German Supercomputing Alliance (HLRN).

*bonitz@theo-physik.uni-kiel.de

- [1] V. E. Fortov, R. I. Ilkaev, V. A. Arinin, V. V. Burtzev, V. A. Golubev, I. L. Iosilevskiy, V. V. Khrustalev, A. L. Mikhailov, M. A. Mochalov, V. Ya. Ternovoi, and M. V. Zhernokletov, Phase Transition in a Strongly Nonideal Deuterium Plasma Generated by Quasi-Isentropic Compression at Megabar Pressures, *Phys. Rev. Lett.* **99**, 185001 (2007).
- [2] T. Dornheim, S. Groth, T. Sjostrom, F. D. Malone, W. M. C. Foulkes, and M. Bonitz, *Ab Initio* Quantum Monte Carlo Simulation of the Warm Dense Electron Gas in the Thermodynamic Limit, *Phys. Rev. Lett.* **117**, 156403 (2016).
- [3] M. Bonitz, C. Henning, and D. Block, Complex plasmas—A laboratory for strong correlations, *Rep. Prog. Phys.* **73**, 066501 (2010).
- [4] U. Schneider, L. Hackermüller, J. P. Ronzheimer, S. Will, S. Braun, T. Best, I. Bloch, E. Demler, S. Mandt, D. Rasch, and A. Rosch, Fermionic transport and out-of-equilibrium dynamics in a homogeneous Hubbard model with ultracold atoms, *Nat. Phys.* **8**, 213 (2012).
- [5] K. Winkler, G. Thalhammer, F. Lang, R. Grimm, J. Hecker Denschlag, A. J. Daley, A. Kantian, H. P. Büchler, and P. Zoller, Repulsively bound atom pairs in an optical lattice, *Nature (London)* **441**, 853 (2006).
- [6] F. Heidrich-Meisner, S. R. Manmana, M. Rigol, A. Muramatsu, A. E. Feiguin, and E. Dagotto, Quantum distillation: Dynamical generation of low-entropy states of strongly correlated fermions in an optical lattice, *Phys. Rev. A* **80**, 041603(R) (2009).
- [7] L. Xia, L. A. Zundel, J. Carrasquilla, A. Reinhard, J. M. Wilson, M. Rigol, and D. S. Weiss, Quantum distillation and confinement of vacancies in a doublon sea, *Nat. Phys.* **11**, 316 (2015).
- [8] N. Schlünzen, S. Hermanns, M. Bonitz, and C. Verdozzi, Dynamics of strongly correlated fermions—*Ab initio* results for two and three dimensions, *Phys. Rev. B* **93**, 035107 (2016).
- [9] M. Schechter and A. Kamenev, Forming doublons by a quantum quench, *Phys. Rev. A* **85**, 043623 (2012).
- [10] D. Greif, L. Tarruell, T. Uehlinger, R. Jördens, and T. Esslinger, Probing Nearest-Neighbor Correlations of Ultracold Fermions in an Optical Lattice, *Phys. Rev. Lett.* **106**, 145302 (2011).
- [11] A. Tokuno, E. Demler, and T. Giamarchi, Doublon production rate in modulated optical lattices, *Phys. Rev. A* **85**, 053601 (2012).
- [12] A. Dirks, K. Mielson, H. R. Krishnamurthy, and J. K. Freericks, Theoretical description of coherent doublon creation via lattice modulation spectroscopy, *Phys. Rev. A* **89**, 021602(R) (2014).
- [13] M. Eckstein, T. Oka, and P. Werner, Dielectric Breakdown of Mott Insulators in Dynamical Mean-Field Theory, *Phys. Rev. Lett.* **105**, 146404 (2010).
- [14] M. Eckstein and P. Werner, Dielectric breakdown of Mott insulators—Doublon production and doublon heating, *J. Phys. Conf. Ser.* **427**, 012005 (2013).
- [15] K. Balzer and M. Eckstein, Field-assisted doublon manipulation in the Hubbard model: A quantum doublon ratchet, *Europhys. Lett.* **107**, 57012 (2014).
- [16] M. Genske and A. Rosch, Directed motion of doublons and holes in periodically driven Mott insulators, *Phys. Rev. A* **90**, 043637 (2014).
- [17] A. V. Joura, J. K. Freericks, and A. I. Lichtenstein, Long-lived nonequilibrium states in the Hubbard model with an electric field, *Phys. Rev. B* **91**, 245153 (2015).
- [18] A. R. Kolovsky and D. N. Maksimov, Mott-insulator state of cold atoms in tilted optical lattices: Doublon dynamics and multilevel Landau-Zener tunneling, *Phys. Rev. A* **94**, 043630 (2016).
- [19] M. Ligges, I. Avigo, D. Golež, H. Strand, L. Stojchevska, M. Källäne, P. Zhou, K. Rossnagel, M. Eckstein, P. Werner, and U. Bovensiepen, Ultrafast Doublon Dynamics in Photo-Excited 1T-TaS₂, *Phys. Rev. Lett.* **120**, 166401 (2018).
- [20] J. P. Covey, S. A. Moses, M. Gärtner, A. Safavi-Naini, M. T. Miecnikowski, Z. Fu, J. Schachenmayer, P. S. Julienne, A. M. Rey, D. S. Jin, and J. Ye, Doublon dynamics and polar molecule production in an optical lattice, *Nat. Commun.* **7**, 11279 (2016).
- [21] M. Bello, C. E. Creffield, and G. Platero, Sublattice dynamics and quantum state transfer of doublons in two-dimensional lattices, *Phys. Rev. B* **95**, 094303 (2017).
- [22] L. Jiao, L. Zhang, X. Wang, G. Diankov, and H. Dai, Narrow graphene nanoribbons from carbon nanotubes, *Nature (London)* **458**, 877 (2009).
- [23] J. Cai, P. Ruffieux, R. Jaafar, M. Bieri, T. Braun, S. Blankenburg, M. Muoth, A. P. Seitsonen, M. Saleh, X. Feng, K. Müllen, and R. Fasel, Atomically precise bottom-up fabrication of graphene nanoribbons, *Nature (London)* **466**, 470 (2010).
- [24] A. Kimouche, M. M. Ervasti, R. Drost, S. Halonen, A. Harju, P. M. Joensuu, J. Sainio, and P. Liljeroth, Ultranarrow metallic armchair graphene nanoribbons, *Nat. Commun.* **6**, 10177 (2015).
- [25] B. V. Senkovskiy, D. Haberer, D. Yu. Usachov, A. V. Fedorov, N. Ehlen, M. Hell, L. Petaccia, G. Di Santo, R. A. Durr, F. R. Fischer, and A. Grüneis, Spectroscopic characterization of $N = 9$ armchair graphene nanoribbons, *Phys. Status Solidi RRL* **11**, 1700157 (2017).
- [26] S. Wang, L. Talirz, C. A. Pignedoli, X. Feng, K. Müllen, R. Fasel, and P. Ruffieux, Giant edge state splitting at atomically precise graphene zigzag edges, *Nat. Commun.* **7**, 11507 (2016).
- [27] L. Talirz, H. Söde, T. Dumsclaff, S. Wang, J. R. Sanchez-Valencia, J. Liu, P. Shinde, C. A. Pignedoli, L. Liang, V. Meunier, N. C. Plumb, M. Shi, X. Feng, A. Narita, K. Müllen, R. Fasel, and P. Ruffieux, On-surface synthesis and characterization of 9-atom wide armchair graphene nanoribbons, *ACS Nano* **11**, 1380 (2017).

- [28] K. Nakada, M. Fujita, G. Dresselhaus, and M. S. Dresselhaus, Edge state in graphene ribbons: Nanometer size effect and edge shape dependence, *Phys. Rev. B* **54**, 17954 (1996).
- [29] Y.-W. Son, M. L. Cohen, and S. G. Louie, Energy Gaps in Graphene Nanoribbons, *Phys. Rev. Lett.* **97**, 216803 (2006).
- [30] P. Ruffieux, J. Cai, N. C. Plumb, L. Patthey, D. Prezzi, A. Ferretti, E. Molinari, X. Feng, K. Müllen, C. A. Pignedoli, and R. Fasel, Electronic structure of atomically precise graphene nanoribbons, *ACS Nano* **6**, 6930 (2012).
- [31] L. Yang, C.-H. Park, Y.-W. Son, M. L. Cohen, and S. G. Louie, Quasiparticle Energies and Band Gaps in Graphene Nanoribbons, *Phys. Rev. Lett.* **99**, 186801 (2007).
- [32] D. Prezzi, D. Varsano, A. Ruini, A. Marini, and E. Molinari, Optical properties of graphene nanoribbons: The role of many-body effects, *Phys. Rev. B* **77**, 041404 (2008).
- [33] A. Ojanperä, A. V. Krashennnikov, and M. Puska, Electronic stopping power from first-principles calculations with account for core electron excitations and projectile ionization, *Phys. Rev. B* **89**, 035120 (2014).
- [34] S. Zhao, W. Kang, J. Xue, X. Zhang, and P. Zhang, Comparison of electronic energy loss in graphene and BN sheet by means of time-dependent density functional theory, *J. Phys. Condens. Matter* **27**, 025401 (2015).
- [35] K. Balzer, N. Schlünzen, and M. Bonitz, Stopping dynamics of ions passing through correlated honeycomb clusters, *Phys. Rev. B* **94**, 245118 (2016).
- [36] E. Gruber, R. A. Wilhelm, R. Petuya, V. Smejkal, R. Kozubek, A. Hierzenberger, B. C. Bayer, I. Aldazabal, A. K. Kazansky, F. Libisch, A. V. Krashennnikov, M. Schleberger, S. Facsko, A. G. Borisov, A. Arnau, and F. Aumayr, Ultrafast electronic response of graphene to a strong and localized electric field, *Nat. Commun.* **7**, 13948 (2016).
- [37] L. D. Landau, Zur theorie der Energieübertragung. II, *Phys. Z. Sowjetunion* **2**, 46 (1932); G. Zener, Non-adiabatic crossing of energy levels, *Proc. R. Soc. A* **137**, 696 (1932).
- [38] F. Hofmann and M. Potthoff, Doublon dynamics in the extended Fermi-Hubbard model, *Phys. Rev. B* **85**, 205127 (2012).
- [39] M. Moeckel and S. Kehrein, Interaction Quench in the Hubbard Model, *Phys. Rev. Lett.* **100**, 175702 (2008).
- [40] M. Eckstein and M. Kollar, Nonthermal Steady States After an Interaction Quench in the Falicov-Kimball Model, *Phys. Rev. Lett.* **100**, 120404 (2008).
- [41] See Supplemental Material at <http://link.aps.org/supplemental/10.1103/PhysRevLett.121.267602> for additional information on the time-dependent Landau-Zener dimer model and additional simulation results that analyze the influence of reduced hopping rates at the edge of finite honeycomb clusters, as well as the effect of long range Coulomb interaction, which includes Ref. [42].
- [42] T. Wassmann, A. P. Seitsonen, A. M. Saitta, M. Lazzeri, and F. Mauri, Structure, Stability, Edge States, and Aromaticity of Graphene Ribbons, *Phys. Rev. Lett.* **101**, 096402 (2008).
- [43] M. Eckstein and P. Werner, Damping of Bloch Oscillations in the Hubbard Model, *Phys. Rev. Lett.* **107**, 186406 (2011).
- [44] R. Rausch and M. Potthoff, Filling-dependent doublon dynamics in the one-dimensional Hubbard model, *Phys. Rev. B* **95**, 045152 (2017).
- [45] K. Balzer and M. Bonitz, *Nonequilibrium Green's Functions Approach to Inhomogeneous Systems*, Lecture Notes in Physics Vol. 867 (Springer, Heidelberg, 2013).
- [46] N. Schlünzen and M. Bonitz, Nonequilibrium Green functions approach to strongly correlated fermions in lattice systems, *Contrib. Plasma Phys.* **56**, 5 (2016).
- [47] N. Schlünzen, J.-P. Joost, F. Heidrich-Meisner, and M. Bonitz, Nonequilibrium dynamics in the one-dimensional Fermi-Hubbard model: A comparison of the nonequilibrium Green functions approach and the density matrix renormalization group method, *Phys. Rev. B* **95**, 165139 (2017).
- [48] M. Kollar, F. A. Wolf, and M. Eckstein, Generalized Gibbs ensemble prediction of prethermalization plateaus and their relation to nonthermal steady states in integrable systems, *Phys. Rev. B* **84**, 054304 (2011).
- [49] E. Canovi, M. Kollar, and M. Eckstein, Stroboscopic prethermalization in weakly interacting periodically driven systems, *Phys. Rev. E* **93**, 012130 (2016).
- [50] M. Rigol, V. Dunjiko, and M. Olshanii, Thermalization and its mechanism for generic isolated quantum systems, *Nature (London)* **452**, 854 (2008).
- [51] M. Cramer, C. M. Dawson, J. Eisert, and T. J. Osborne, Exact Relaxation in a Class of Nonequilibrium Quantum Lattice Systems, *Phys. Rev. Lett.* **100**, 030602 (2008).
- [52] I. Adamovich, S. D. Baalrud, A. Bogaerts, P. J. Bruggeman, M. Cappelli, V. Colombo, U. Czarnetzki, U. Ebert, J. G. Eden, P. Favia *et al.*, The 2017 plasma roadmap: Low temperature plasma science and technology, *J. Phys. D* **50**, 323001 (2017).
- [53] Z. Idziaszek, T. Calarco, P. S. Julienne, and A. Simoni, Quantum theory of ultracold atom-ion collisions, *Phys. Rev. A* **79**, 010702(R) (2009).
- [54] C. Weitenberg, M. Endres, J. F. Sherson, M. Cheneau, P. Schauß, T. Fukuhara, I. Bloch, and S. Kuhr, Single-spin addressing in an atomic Mott insulator, *Nature (London)* **471**, 319 (2011).